Compensation of Tool Deflection in Robotic-based Milling

Alexandr Klimchik[1,2], Dmitry Bondarenko[2,3], Anatol Pashkevich[1,2],
Sebastien Briot[2] and Benôit Furet[2,4]

[1]*Ecole des Mines de Nantes, 4 Rue Alfred-Kastler, 44307, Nantes, France*
[2]*Institut de Recherches en Communications et Cybernétique de Nantes, UMR CNRS 6597, Nantes, France*
[3]*Ecole Centrale de Nantes, 1 Rue de la Noë, 44 321, Nantes, France*
[4]*Université de Nantes, Quai de Tourville, 44035, Nantes, France*

Abstract: The paper presents the compliance errors compensation technique for industrial robots, which are used in milling manufacturing cells. under external loading, which is based on the non-linear stiffness model. In contrast to previous works, it takes into account the interaction between the milling tool and the workpiece that depends on the end-effector position, process parameters and cutting conditions (spindle rotation, feed rate, geometry of the tool, etc.). Within the developed technique, the compensation errors caused by external loading is based on the non-linear stiffness model and reduces to a proper adjusting of a target trajectory that is modified in the off-line mode. The advantages and practical significance of the proposed technique are illustrated by an example that deals with milling with Kuka robot.

1 INTRODUCTION

Currently, robots become more and more popular for a variety of technological processes, including high-speed precision machining. For this process, the robot is subjected by external loading which caused by the machining force. This force is generated by the interaction between the tool mounted on the robot end-effector and the workpiece during the material removal (Dépincé, 2006). It is a contact force and it is distributed along the affected area of the tool cutting part. To evaluate the influence and to analyze the robot behavior while machining, the cutting force should be defined either experimentally or using accurate mathematical model.

To evaluate the force caused by interaction between the tool and the workpiece, two approaches can be used. The static approach allows computing the average cutting force without any consideration of dynamic aspect in machining system. This force serves as an external loading of the robot. This approach is widely used in analysis of conventional machining processes using CNC machines (Altintas, 2000), where the stiffness is high. In contrast, robots have relatively low structural stiffness. For this rea-

son, in the case of robotic-based machining, an additional source of dynamic displacements of the end-effector with respect to the desired trajectory induced by robot compliance may arise. Such behavior leads to the variable contact between the machining tool and the workpiece. Thus, the generated contact force depends on the current position of the robot end-effector on the trajectory. Consequently, the cutting force cannot be evaluated correctly using the static approach. In this case, the dynamic approach, which will be used in the paper, is required. It is based on computing of the force at each instant of machining process that defines loading of the robot for the next instant of processing. As a result, the dynamic aspect of robot motion under such variable cutting force can be examined for whole process.

Usually, in the robot-based machining this force causes essential deflections that decrease the quality of the final product. The problem of the robot error compensation can be solved in two ways that differ in degree of modification of the robot control software:

(a) by *modification of the manipulator model,* which better suits to the real manipulator and is used by the robot controller (in simple case, it can be limited by tuning of the nominal manipulator model, but

may also involve essential model enhancement by introducing additional parameters, if it is allowed by a robot manufacturer);

(b) by *modification of the robot control program* that defines the prescribed trajectory in Cartesian space (here, using relevant error model, the input trajectory is generated in such way that under the loading the output trajectory coincides with the desired one, while input trajectory differs from the target one).

Moreover, with regard to the robot-based machining, there is a solution that does not require force/torque measurements or computations (Dépincé, 2006), where the target trajectory for the robot controller is modified by applying the "mirror" technique. An evident advantage of this technique is its applicability to the compensation of all types of the robot errors, including geometrical and compliance ones. However, this approach requires carrying out additional preliminary experiments which are quite expensive. So, it is suitable for the large-scale production only. Another compensation methodology has been proposed by Eastwood and Webb (Eastwood, 2010) that was used for gravitational deflection compensation for hybrid parallel kinematic machines.

This paper focuses on the modification of control program that is considered to be more realistic in practice. This approach requires also accurate stiffness model of the manipulator. From point of view of stiffness analysis, the external and forces directly influence on the manipulator equilibrium configuration and, accordingly, may modify the stiffness properties. So, they must be undoubtedly taken into account while developing the stiffness model. However, in most of the related works the Cartesian stiffness matrix has been computed for the nominal configuration (Chen, 2000; Alici, 2005). Such approach is suitable for the case of small deflections only. For the opposite case, the most important results have been obtained in (Kövecses, 2007; Tyapin, 2009; Pashkevich, 2011), which deal with the stiffness analysis of manipulators under the end-point loading.

Thus, to compensate errors caused by the machining process, it is required to have an accurate stiffness model and precise cutting force model. In contrast to the previous works, the compliance error compensation technique presented in this work is based on the non-linear stiffness model of the manipulator (Pashkevich, 2011) and dynamic model of technological process that generates the cutting force.

2 PROBLEM STATEMENT

For the *compliance errors*, the compensation technique must rely on two components. The first of them describes distribution of the stiffness properties throughout the workspace and is defined by the stiffness matrix as a function of the joint coordinates. The second component describes the forces/torques acting on the end-effector while the manipulator is performing its machining task (manipulator *loading*).

The *stiffness matrix* required for the compliance errors compensation highly depends on the robot configuration and essentially varies throughout the workspace. From general point of view, full-scale compensation of the compliance errors requires essential revision of the manipulator model embedded in the robot controller. In fact, instead of conventional geometrical model that provides inverse/direct coordinate transformations from the joint to Cartesian spaces and vice versa, here it is necessary to employ the so-called *kinetostatic model* (Su, 2006). It is essentially more complicated than the geometrical model and requires rather intensive computations that are presented in Section 3..

The dynamic behavior of the robot under the loading **F** caused by technological process can be described as

$$\mathbf{M}_C \delta \ddot{\mathbf{t}} + \mathbf{C}_C \delta \dot{\mathbf{t}} + \mathbf{K}_C \delta \mathbf{t} = \mathbf{F} \qquad (1)$$

where $\mathbf{M}_C$ is 6×6 mass matrix that represents the global behavior of the robot in terms of natural frequencies, $\mathbf{C}_C$ is 6×6 damping matrix, $\mathbf{K}_C$ is 6×6 Cartesian stiffness matrix of the robot under the external loading **F**, $\delta \mathbf{t}, \delta \dot{\mathbf{t}}$ and $\delta \ddot{\mathbf{t}}$ are dynamic displacement, velocity and acceleration of the tool endpoint in a current moment respectively (Briot, 2011).

In general, the cutting force F_c has a *nonlinear* nature and depends on many factors such as cutting conditions, properties of workpiece material and tool cutting part, etc (Ritou, 2006). But, for given tool/workpiece combination, the force F_c could be approximated *as a function* of an uncut chip thickness h, which represents the desired thickness to cut at each instant of machining.

Hence, to reduce errors caused by cutting forces in the robotic-based machining it is required to obtain an accurate elasto-static model of robot and elasto-dynamic model of machining process. These problems are addressed in the following sections taking into account some particularities of the considered application (robotic-based milling).

3 MANIPULATOR MODEL

3.1 Elasto-Static Model

Elasto-static model of a serial robot is usually de-fined by its Cartesian stiffness matrix, which should be computed in the neighborhood of loaded configu-ration. Let us propose numerical technique for com-puting static equilibrium configuration for a general type of serial manipulator. Such manipulator may be approximated as a set of rigid links and virtual joints, which take into account elasto-static proper-ties (Figure 1). Since the link weight of serial robots is not negligible, it is reasonable to decompose it in-to two parts (based on the link mass centre) and ap-ply them to the both ends of the link. All this load-ings will be aggregated in a vector $\mathbf{G} = [\mathbf{G}_1 ... \mathbf{G}_n]$, where $\mathbf{G}_i$ is the loading applied to the i-th node-point. Besides, it is assumed that the external load-ing $\mathbf{F}$ (caused by the interaction of the tool and the workpiece) is applied to the robot end-effector.
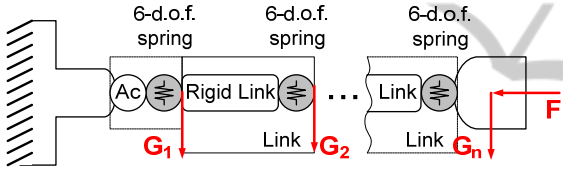

Figure 1: VJM model of industrial robot with end-point and auxiliary loading.

Following the principle of virtual work, the work of external forces $\mathbf{G}$, $\mathbf{F}$ is equal to the work of inter-nal forces $\mathbf{\tau}_\theta$ caused by displacement of the virtual springs $\delta\mathbf{\theta}$

$$\sum_{j=1}^{n} \left(\mathbf{G}_j^{\mathrm{T}} \cdot \delta\mathbf{t}_j \right) + \mathbf{F}^{\mathrm{T}} \cdot \delta\mathbf{t} = \mathbf{\tau}_\theta^{\mathrm{T}} \cdot \delta\mathbf{\theta} \qquad (2)$$

where the virtual displacements $\delta\mathbf{t}_j$ can be comput-ed from the linearized geometrical model derived from $\delta\mathbf{t}_j = \mathbf{J}_\theta^{(j)} \delta\mathbf{\theta}$, $j = 1..n$, which includes the Jaco-bian matrices $\mathbf{J}_\theta^{(j)} = \partial\mathbf{g}_j(\mathbf{q}, \mathbf{\theta})/\partial\mathbf{\theta}$ with respect to the virtual joint coordinates.

So, expression (2) can be rewritten as

$$\sum_{j=1}^{n} \left(\mathbf{G}_j^{\mathrm{T}} \cdot \mathbf{J}_\theta^{(j)} \cdot \delta\mathbf{\theta} \right) + \left(\mathbf{F}^{\mathrm{T}} \cdot \mathbf{J}_\theta^{(n)} \cdot \delta\mathbf{\theta} \right) = \mathbf{\tau}_\theta^{\mathrm{T}} \cdot \delta\mathbf{\theta} \qquad (3)$$

which has to be satisfied for any variation of $\delta\mathbf{\theta}$. It means that the terms regrouping the variables $\delta\mathbf{\theta}$ have the coefficients equal to zero. Hence the force

balance equations can be written as

$$\mathbf{\tau}_\theta = \sum_{j=1}^{n} \mathbf{J}_\theta^{(j)\mathrm{T}} \cdot \mathbf{G}_j + \mathbf{J}_\theta^{(n)\mathrm{T}} \cdot \mathbf{F} \qquad (4)$$

These equations can be re-written in block-matrix form as

$$\mathbf{\tau}_\theta = \mathbf{J}_\theta^{(G)\mathrm{T}} \cdot \mathbf{G} + \mathbf{J}_\theta^{(F)\mathrm{T}} \cdot \mathbf{F} \qquad (5)$$

where $\mathbf{J}_\theta^{(F)} = \mathbf{J}_\theta^{(n)}$, $\mathbf{J}_\theta^{(G)} = \left[\mathbf{J}_\theta^{(1)\mathrm{T}} ... \mathbf{J}_\theta^{(n)\mathrm{T}} \right]^{\mathrm{T}}$, $\mathbf{G} = \left[\mathbf{G}_1^{\mathrm{T}} ... \mathbf{G}_n^{\mathrm{T}} \right]^{\mathrm{T}}$. Finally, taking into account the virtual spring reaction $\mathbf{\tau}_\theta = \mathbf{K}_\theta \cdot \mathbf{\theta}$, where $\mathbf{K}_\theta = diag\left(\mathbf{K}_{\theta_1}, ..., \mathbf{K}_{\theta_n} \right)$, the desired static equilibri-um equations can be presented as

$$\mathbf{J}_\theta^{(G)\mathrm{T}} \cdot \mathbf{G} + \mathbf{J}_\theta^{(F)\mathrm{T}} \cdot \mathbf{F} = \mathbf{K}_\theta \cdot \mathbf{\theta} \qquad (6)$$

To obtain a relation between the external loading $\mathbf{F}$ and internal coordinates of the kinematic chain $\mathbf{\theta}$ corresponding to the static equilibrium, equations (6) should be solved either for different given values of $\mathbf{F}$ or for different given values of $\mathbf{t}$. Let us solve the static equilibrium equations with respect to the ma-nipulator configuration $\mathbf{\theta}$ and the external loading $\mathbf{F}$ for given end-effector position $\mathbf{t} = \mathbf{g}(\mathbf{\theta})$ and the function of auxiliary-loadings $\mathbf{G}(\mathbf{\theta})$

$$\mathbf{K}_\theta \cdot \mathbf{\theta} = \mathbf{J}_\theta^{(G)\mathrm{T}} \mathbf{G} + \mathbf{J}_\theta^{(F)\mathrm{T}} \mathbf{F}; \quad \mathbf{t} = \mathbf{g}(\mathbf{\theta}); \quad \mathbf{G} = \mathbf{G}(\mathbf{\theta}) \qquad (7)$$

where the unknown variables are $(\mathbf{\theta}, \mathbf{F})$.

Since usually this system has no analytical solu-tion, iterative numerical technique can be applied. So, the kinematic equations may be linearized in the neighborhood of the current configuration $\mathbf{\theta}_i$

$$\mathbf{t}_{i+1} = \mathbf{g}(\mathbf{\theta}_i) + \mathbf{J}_\theta^{(F)}(\mathbf{\theta}_i) \cdot (\mathbf{\theta}_{i+1} - \mathbf{\theta}_i); \qquad (8)$$

where the subscript 'i' indicates the iteration number and the changes in Jacobians $\mathbf{J}_\theta^{(G)}$, $\mathbf{J}_\theta^{(F)}$ and the auxil-iary loadings $\mathbf{G}$ are assumed to be negligible from iteration to iteration. Correspondingly, the static equilibrium equations in the neighborhood of $\mathbf{\theta}_i$ may be rewritten as

$$\mathbf{J}_\theta^{(G)\mathrm{T}} \cdot \mathbf{G} + \mathbf{J}_\theta^{(F)\mathrm{T}} \cdot \mathbf{F}_{i+1} = \mathbf{K}_\theta \cdot \mathbf{\theta}_{i+1}. \qquad (9)$$

Thus, combining (8), (9) and analytical expression for $\mathbf{\theta} = \mathbf{K}_\theta^{-1}(\mathbf{J}_\theta^{(G)\mathrm{T}} \cdot \mathbf{G} + \mathbf{J}_\theta^{(F)\mathrm{T}} \cdot \mathbf{F})$, the unknown varia-bles $\mathbf{F}$ and $\mathbf{\theta}$ can be computed using following itera-tive scheme

$$\mathbf{F}_{i+1} = \left(\mathbf{J}_{\theta}^{(\mathrm{F})} \cdot \mathbf{K}_{\theta}^{-1} \cdot \mathbf{J}_{\theta}^{(\mathrm{F})\mathrm{T}}\right)^{-1} \cdot$$
$$\left(\mathbf{t}_{i+1} - \mathbf{g}(\mathbf{\theta}_i) + \mathbf{J}_{\theta}^{(\mathrm{F})}\mathbf{\theta}_i - \mathbf{J}_{\theta}^{(\mathrm{F})}\mathbf{K}_{\theta}^{-1}\mathbf{J}_{\theta}^{(\mathrm{G})\mathrm{T}}\mathbf{G}_i\right) \quad (10)$$
$$\mathbf{\theta}_{i+1} = \mathbf{K}_{\theta}^{-1}\left(\mathbf{J}_{\theta}^{(\mathrm{G})\mathrm{T}} \cdot \mathbf{G}_i + \mathbf{J}_{\theta}^{(\mathrm{F})\mathrm{T}} \cdot \mathbf{F}_{i+1}\right)$$

The proposed algorithm allows us to compute the static equilibrium configuration for the serial robot under external loadings applied to any point of the manipulator and the loading from the technological process.

3.2 Stiffness Matrix

In order to obtain the Cartesian stiffness matrix, let us linearize the force-deflection relation in the neighborhood of the equilibrium. Following this approach, two equilibriums that correspond to the manipulator state variables $(\mathbf{F}, \mathbf{\theta}, \mathbf{t})$ and $(\mathbf{F} + \delta\mathbf{F}, \mathbf{\theta} + \delta\mathbf{\theta}, \mathbf{t} + \delta\mathbf{t})$ should be considered simultaneously. Here, notations $\delta\mathbf{F}$, $\delta\mathbf{t}$ define small increments of the external loading and relevant displacement of the end-point. Finally, the static equilibrium equations may be written as

$$\mathbf{t} = \mathbf{g}(\mathbf{\theta}); \qquad \mathbf{K}_{\theta} \cdot \mathbf{\theta} = \mathbf{J}_{\theta}^{(\mathrm{G})\mathrm{T}} \cdot \mathbf{G} + \mathbf{J}_{\theta}^{(\mathrm{F})\mathrm{T}} \cdot \mathbf{F} \quad (11)$$

and

$$\mathbf{t} + \delta\mathbf{t} = \mathbf{g}(\mathbf{\theta} + \delta\mathbf{\theta})$$
$$\mathbf{K}_{\theta} \cdot (\mathbf{\theta} + \delta\mathbf{\theta}) = \left(\mathbf{J}_{\theta}^{(\mathrm{G})} + \delta\mathbf{J}_{\theta}^{(\mathrm{G})}\right)^{\mathrm{T}} \cdot (\mathbf{G} + \delta\mathbf{G}) \quad (12)$$
$$+ \left(\mathbf{J}_{\theta}^{(\mathrm{F})} + \delta\mathbf{J}_{\theta}^{(\mathrm{F})}\right)^{\mathrm{T}} \cdot (\mathbf{F} + \delta\mathbf{F})$$

where $\mathbf{t}, \mathbf{F}, \mathbf{G}, \mathbf{K}_{\theta}, \mathbf{\theta}$ are assumed to be known.

After linearization of the function $\mathbf{g}(\mathbf{\theta})$ in the neighborhood of the loaded equilibrium, the system (11), (12) is reduced to equations

$$\delta\mathbf{t} = \mathbf{J}_{\theta}^{(\mathrm{F})}\delta\mathbf{\theta}$$
$$\mathbf{K}_{\theta} \cdot \delta\mathbf{\theta} = \delta\mathbf{J}_{\theta}^{(\mathrm{G})}\mathbf{G} + \mathbf{J}_{\theta}^{(\mathrm{G})}\delta\mathbf{G} + \delta\mathbf{J}_{\theta}^{(\mathrm{F})}\mathbf{F} + \mathbf{J}_{\theta}^{(\mathrm{F})}\delta\mathbf{F} \quad (13)$$

which defines the desired linear relations between $\delta\mathbf{t}$ and $\delta\mathbf{F}$. In this system, small variations of Jacobians may be expressed via the second order derivatives $\delta\mathbf{J}_{\theta}^{(\mathrm{F})} = \mathbf{H}_{\theta\theta}^{(\mathrm{F})} \cdot \delta\mathbf{\theta}$, $\delta\mathbf{J}_{\theta}^{(\mathrm{G})} = \mathbf{H}_{\theta\theta}^{(\mathrm{G})} \cdot \delta\mathbf{\theta}$, where $\mathbf{H}_{\theta\theta}^{(\mathrm{G})} = \sum_{j=1}^{n} \partial^2 \mathbf{g}_j^T \mathbf{G}_j / \partial\mathbf{\theta}^2$, $\mathbf{H}_{\theta\theta}^{(\mathrm{F})} = \partial^2 \mathbf{g}^T \mathbf{F}/\partial\mathbf{\theta}^2$. Also, the auxiliary loading $\mathbf{G}$ may be computed via the first order derivatives as $\delta\mathbf{G} = \partial\mathbf{G}/\partial\mathbf{\theta} \cdot \delta\mathbf{\theta}$

Further, let us introduce additional notation $\mathbf{H}_{\theta\theta} = \mathbf{H}_{\theta\theta}^{(\mathrm{F})} + \mathbf{H}_{\theta\theta}^{(\mathrm{G})} + \mathbf{J}_{\theta}^{(\mathrm{G})\mathrm{T}} \cdot \partial\mathbf{G}/\partial\mathbf{\theta}$, which allows us to present system (13) in the form

$$\begin{bmatrix} \delta\mathbf{t} \\ \mathbf{0} \end{bmatrix} = \begin{bmatrix} \mathbf{0} & \mathbf{J}_{\theta}^{(\mathrm{F})} \\ \mathbf{J}_{\theta}^{(\mathrm{F})\mathrm{T}} & -\mathbf{K}_{\theta} + \mathbf{H}_{\theta\theta} \end{bmatrix} \cdot \begin{bmatrix} \delta\mathbf{F} \\ \delta\mathbf{\theta} \end{bmatrix} \quad (14)$$

So, the desired Cartesian stiffness matrices $\mathbf{K}_{\mathrm{C}}$ can be computed as

$$\mathbf{K}_{\mathrm{C}} = \left(\mathbf{J}_{\theta}^{(\mathrm{F})}(\mathbf{K}_{\theta} - \mathbf{H}_{\theta\theta})^{-1}\mathbf{J}_{\theta}^{(\mathrm{F})\mathrm{T}}\right)^{-1} \quad (15)$$

Below, this expression will be used for computing of the elasto-static deflections of the robotic manipulator.

3.3 Mass Matrix

To evaluate dynamic behaviour of the robot under the loading, in addition to the Cartesian stiffness matrix $\mathbf{K}_{\mathrm{C}}$ it is required to define the mass matrix $\mathbf{M}_{\mathrm{C}}$. Comprehensive analysis and definition of this matrix have been proposed in (Briot, 2011). Here, let us summarise the main results that will be used further in the error compensation technique.

Similar to the stiffness matrix, here physical properties defined by the mass matrix $\mathbf{M}_{\mathrm{C}}$ are constant in the joint coordinates $\mathbf{M}_{\theta} = const$ and are defined by the mass matrices $\mathbf{M}_{\theta i}$ of all n links of the robot $\mathbf{M}_{\theta} = diag(\mathbf{M}_{\theta 1}, ..., \mathbf{M}_{\theta n})$. Assuming that link may be approximated by a beam with a constant cross-section, the mass matrix $\mathbf{M}_{\theta i}$ can be computed as

$$\mathbf{M}_{\theta i} = diag(a_1, a_2, a_3, a_4, a_5, a_6) \quad (16)$$

where $a_1 = m_i / 3$, $a_2 = 33m_i / 140$, $a_3 = 33m_i / 140$, $a_4 = I_i^p \rho_i L_i / 3$, $a_5 = 8I_i^y \rho_i L_i / 15$, $a_6 = 8I_i^z \rho_i L_i / 15$, m_i is physical mass of i-th link, ρ_i is density of i-th link, L_i is link length, I_i^p is the polar moment, I_i^y, I_i^z are the second moments of the area. Since the mass matrix $\mathbf{M}_{\theta}$ is defined in the joint coordinates it can be recomputed into the Cartesian coordinates associated with the tool end-point using the Jacobian matrix $\mathbf{J}_{\theta}$ (which depend on the robot configuration $\mathbf{q}$ and computed with respect to virtual joint coordinates $\mathbf{\theta}$) using following expression

$$\mathbf{M}_{\mathrm{C}} = \mathbf{J}_{\theta}^{T}\mathbf{M}_{\theta}\mathbf{J}_{\theta} \quad (17)$$

Thus, using expressions (16) and (17) it is possible to compute the mass matrix $\mathbf{M}_{\mathrm{C}}$ for a given robot configuration $\mathbf{q}$.

4 MACHINING PROCESS

Let us obtain the model of the cutting force which depends on the relative position of the tool with respect to the workpiece at each instant of machining. As follows from previous works (Brissaud, 2008), for the known chip thickness *h,* the cutting force F_c can be expresses as

$$F_c(h) = k_0 \frac{h/h_s + r(h/h_s)^2}{1 + h/h_s} a_p, \quad h \geq 0 \qquad (18)$$

where a_p is a depth of cut, $r = k_\infty/k_0 < 1$ depends on the parameters k_∞, k_0 that define the so called stiffness of the cutting process for large and small chip thickness *h* respectively (Figure 2) and h_s is a specific chip thickness, which depends on the current state of the tool cutting edge. The parameters k_0, h_s, r are evaluated experimentally for a given combination of tool/working material. To take into account the possible loss of contact between the tool and the workpiece, expression (18) should be supplement by the case of $h < 0$ as
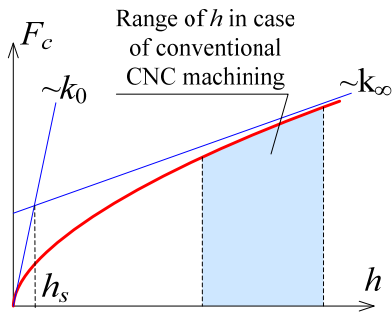
Figure 2: Fractional cutting force model $F_c(h)$.

$$F_c(h) = 0, \quad \text{if} \quad h < 0 \qquad (19)$$

For the multi-edge tool the machining surface is formed by means of several edges simultaneously. The number of working edges varies during machining and depends on the width of cut. For this reason, the total force F_c of such interaction is a superposition of forces $F_{c,i}$ generated by each tool edge *i*, which are currently in the contact with the workpiece. Besides, the contact force $F_{c,i}$ can be decomposed by its *radial* $F_{r,i}$ and *tangential* $F_{t,i}$ components (Figure 3). In accordance with Merchant's model (Merchant, 1945), the *t*-component of cutting force $F_{t,i}$ can be computed with the equation (18). The *r*-component $F_{r,i}$ is related with $F_{t,i}$ by following expression (Laporte 2009)

$$F_{r,i} = k_r F_{t,i} \qquad (20)$$

where the ratio factor k_r depends on the given tool/workpiece characteristics.

It should be mentioned that in robotic machining it is more suitable to operate with forces expressed in the robot tool frame $\{x,y,z\}$. Then, the corresponding components F_x, F_y (Figure 3) of the cutting force F_c can be expressed as follows

$$F_x = \sum_{i=1}^{n_z} -F_{r,i} \cos \varphi_i + \sum_{i=1}^{n_z} F_{t,i} \sin \varphi_i$$
$$F_y = \sum_{i=1}^{n_z} F_{r,i} \sin \varphi_i + \sum_{i=1}^{n_z} F_{t,i} \cos \varphi_i \qquad (21)$$

where n_z is the number of currently working cutting edges, φ_i is the angular position of the *i*-th cutting edge (the cutting force in *z* direction F_z is negligible here). So, the vector of external loading of the robot due to the machining process can be composed in the frame $\{x,y,z\}$ using the defined components F_x, F_y as $\mathbf{F} = [F_x, F_y, 0, 0, 0, 0]^T$.
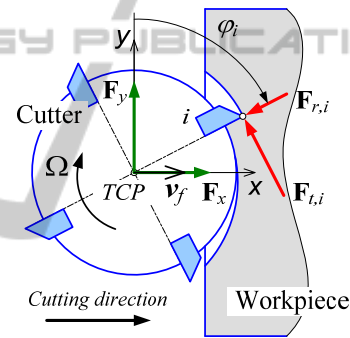

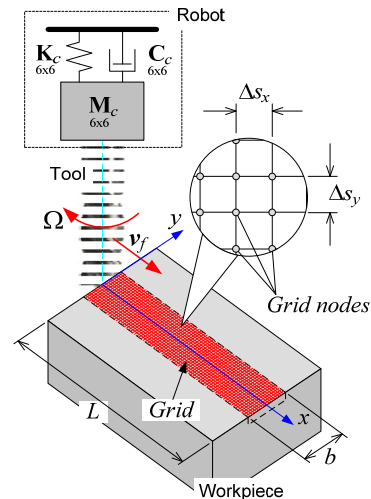Figure 3: Forces of tool/workpiece interaction.

Figure 4: Meshing of the workpiece area.

It should be stressed that the cutting force compo-

nents $F_{r,i}$, $F_{t,i}$ mentioned in equation (18),(20) are computed for the given chip thickness h_i, which should be also evaluated. Let us define model for h_i using mechanical approach. Then the chip thickness h_i removed by i-th tooth depends on the angular position φ_i of this tooth and it can be evaluated using to the geometrical distance between the position of the given tooth i and the current machining profile (Figure 3). It should be mentioned, that the main issue here is to follow the current relative position between the i-th tooth and the working material or to define whether the i-th tooth is involved in cutting for given instant of process. Because of the robot dynamic behavior and the regenerative mechanism of surface formation (Tlusty, 1981) this problem cannot be solved directly using kinematic relations. In this case it is reasonable to introduce a special rectangular grid, which decomposes the workpiece area into segments and allows tracking the tool/workpiece interaction and the formation of the machining profile (Figure 4).

Here, Steps Δs_x, Δs_y between grid nodes are constant and depend on the tool geometry, cutting condition and time discretization $\Delta \tau$. Each node j ($j = \overline{1, N_w}$, N_w is the number of nodes) of the grid can be marked as "1" or "0": "1" corresponds to nodes situated in the workpiece area with material (rose nodes in 0), "0" corresponds to nodes situated in workpiece area that was cut away (white nodes in 0).

In order to define the number of currently cut nodes by the i-th tooth, the previous instant of machining process should be considered. Let us define A_i as an amount of working material that is currently cut away by the i-th tooth (Figure 5). So, if node j marked as "1" is located inside the marked sector (green nodes in Figure 5), it changes to "0" and A_i is increasing by $\Delta s_x \Delta s_y$. Analyzing all potential nodes and computing A_i, the chip thickness h_i, removed at given instant of the process by the i-th tooth, can be estimated by $h_i = A_i / R \Delta \alpha_i$, $i = \overline{1, N_z}$. The angle $\Delta \varphi_i$ determines the current angular position of the i-th tooth regarding to its position at the instant τ-$\Delta\tau$ and referred to the position of TCP at τ-$\Delta\tau$.

Described mechanism of chip formation and the machining force model (18) allow computing the dynamic behavior of the robotic machining process where models of robot inertia and stiffness are discussed in the section 3 of the paper. The detailed algorithm that is used in numerical analysis is presented in Figure 6, where the analysis of the robot dynamics is performed in the tool frame with respect to the dynamic displacement of the tool δt_{dyn} fixed on the robot end-effector around its position on the trajectory..
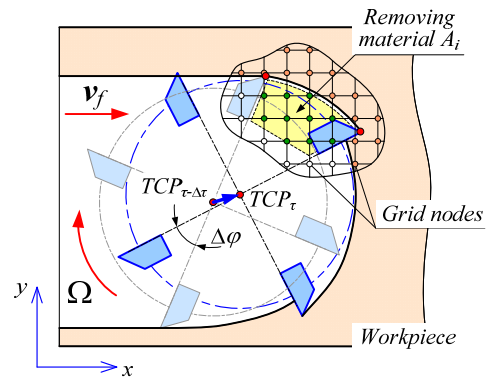

Figure 5: Evaluating the tool/workpiece intersection A_i and computing the corresponding chip thickness h_i.
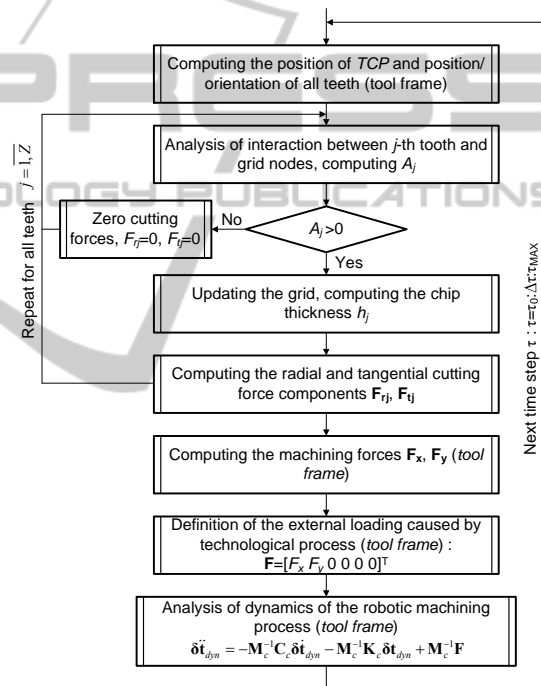

Figure 6: Algorithm for numerical simulation of robotic machining process dynamics.

5 COMPLIANCE ERROR COMPENSATION TECHNIQUE

In industrial robotic controllers, the manipulator motions are usually generated using the inverse kinematic model that allows us to compute the input signals for actuators $\boldsymbol{\rho}_0$ corresponding to the desired end-effector location $\mathbf{t}_0$, which is assigned assuming that the compliance errors are negligible. However, if the external loading $\mathbf{F}$ is essential, the kin-

ematic control becomes non-applicable because of changes in the end-effector location. It can be computed from the non-linear compliance model as

$$\mathbf{t}_{\mathrm{F}} = f^{-1}\left(\mathbf{F} \mid \mathbf{t}_0\right) \qquad (22)$$

where the subscripts 'F' and '0' refer to the loaded and unloaded modes respectively, and '|' separates arguments and parameters of the function $f(\ )$. Some details concerning this function are given in our previous publication (Pashkevich, 2011).

To compensate this undeterred end-effector displacement from $\mathbf{t}_0$ to $\mathbf{t}_{\mathrm{F}}$, the target point should be modified in such a way that, under the loading $\mathbf{F}$, the end-platform is located in the desired point $\mathbf{t}_0$. This requirement can be expressed using the stiffness model in the following way

$$\mathbf{F} = f\left(\mathbf{t}_0 \mid \mathbf{t}_0^{(\mathrm{F})}\right) \qquad (23)$$

where $\mathbf{t}_0^{(\mathrm{F})}$ denotes the modified target location. Hence, the problem is reduced to the solution of the nonlinear equation (23) for $\mathbf{t}_0^{(\mathrm{F})}$, while $\mathbf{F}$ and $\mathbf{t}_0$ are assumed to be given. It is worth mentioning that this equation completely differs from the equation $\mathbf{F} = f(\mathbf{t} \mid \mathbf{t}_0)$, where the unknown variable is $\mathbf{t}$. It means that here the compliance model does not allow us to compute the modified target point $\mathbf{t}_0^{(\mathrm{F})}$ straightforwardly, while the linear compensation technique directly operates with Cartesian compliance matrix (Gong, 2000).

To solve equation (23) for $\mathbf{t}_0^{(\mathrm{F})}$, similar numerical technique can be applied. It yields the following iterative scheme

$$\mathbf{t}_0^{(\mathrm{F})\prime} = \mathbf{t}_0^{(\mathrm{F})} + \alpha \cdot \left(\mathbf{t}_0 - f^{-1}(\mathbf{F} \mid \mathbf{t}_0^{(\mathrm{F})})\right) \qquad (24)$$

where the prime corresponds to the next iteration, $\alpha \in (0,1)$ is the scalar parameter ensuring the convergence. More detailed presentation of the developed iterative routines is given in Figure 7.
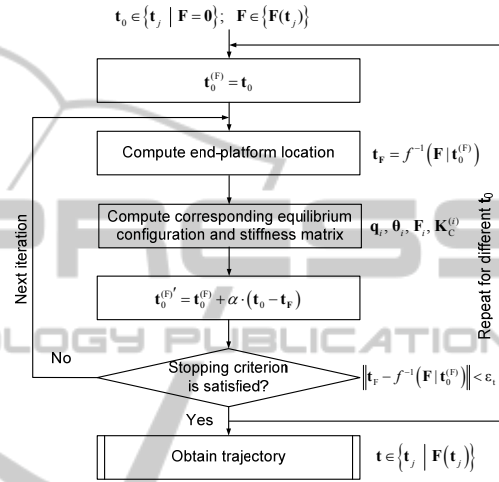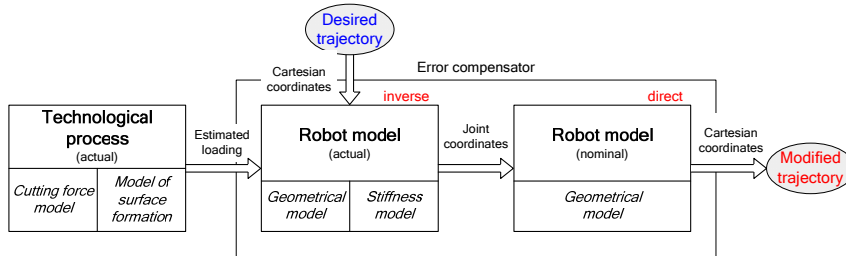

Figure 7: Procedure for compensation of compliance errors.

Hence, using the proposed computational techniques, it is possible to compensate a main part
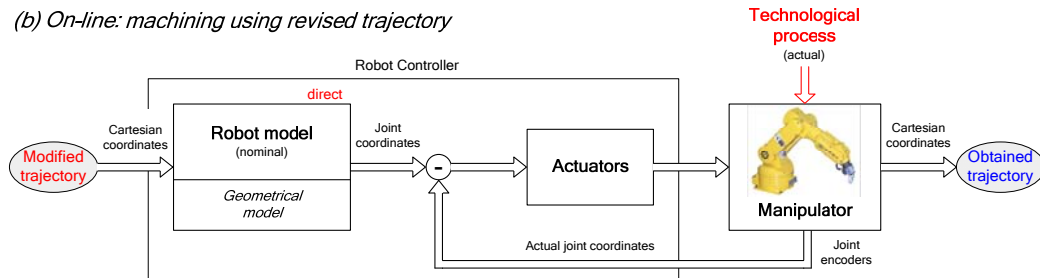

Figure 8: Implementation of compliance error compensation technique.

compliance errors by proper adjusting the reference trajectory that is used as an input for robotic controller. In this case, the control is based on the inverse kinetostatic model (instead of kinematic one) that takes into account both the manipulator geometry and elastic properties of its links and joints. Implementation of developed compliance error compensation technique presented in Figure 8.

6 EXPERIMENTAL VERIFICATION

The developed compliance error compensation technique has been verified experimentally for robotic milling with the KUKA KR270 robot along a simple trajectory in aluminum workpiece. It is assumed that at the beginning of the technological process the robot is in the configuration **q** (see Table 1 Figure 9). The parameters of the stiffness model for the considered robot have been identified in (Dumas, 2011) and are presented in Table 1. Link masses required for the mass matrix of the robot are presented also in Table 1.

Table 1: Initial data for robotic-based milling.

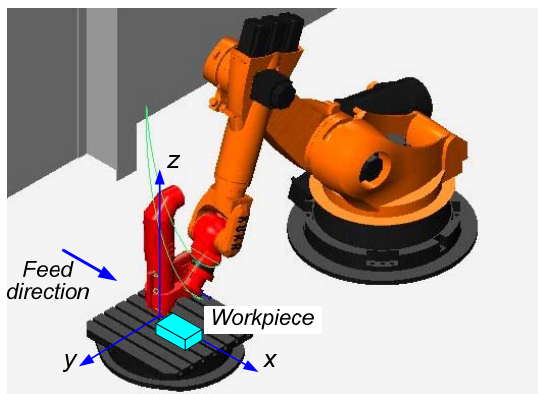| Joint coordinates, [deg]					
q_1	q_2	q_3	q_4	q_5	q_6
90	-50	120	180	25	180
Joint compliances, [rad/N m]*10^{-6}					
k_1	k_2	k_3	k_4	k_5	k_6
0.26	0.15	0.26	1.79	1.52	2.13
Link masses, [kg]					
m_1	m_2	m_3	m_4	m_5	m_6
336.8	259.4	85.2	54.5	36.3	18.2

Figure 9: Starting pose of the KUKA KR270 robot to perform the operation of milling.

For the milling, the cutter with the external diameter D=20 mm and four teeth (N_z=4) distributed uniformly over the tool is used. For the given combination of the tool and the workpiece material the following parameters correspond to the cutting force model defined in (18): k_0=5×10^6 N/m, h_s=1.8×10^{-5} m, r=0.1, k_r=0.3.
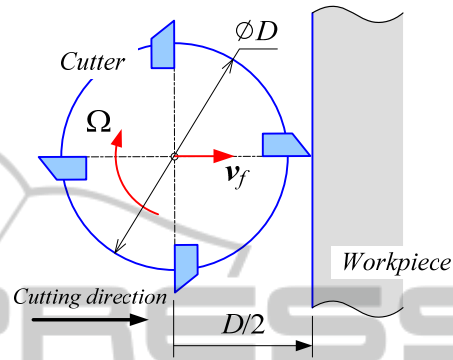

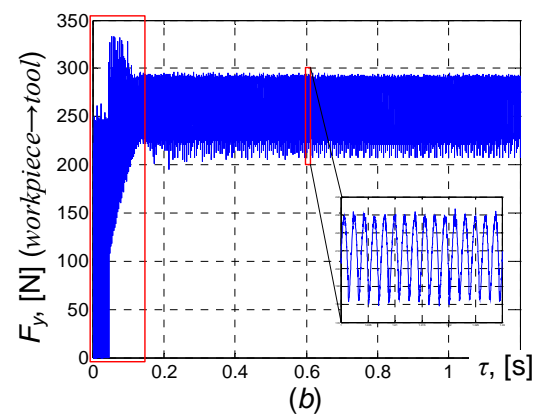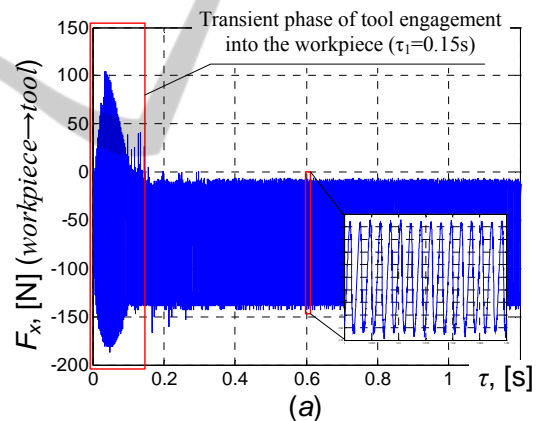Figure 10: Starting relative position of the tool with respect to the workpiece.

Figure 11: Variation of machining force components F_x (*a*) and F_y (*b*) for whole milling process.

Taking into account that the workpiece has a straight borders let us assume that at the instant t=0 one of the teeth of the tool is in contact with the workpiece material as it is shown in the Figure 10. It is also assumed that the machining process is performing with the constant feed rate v_f=4 m/min (applied in x-direction of the robot tool frame) and the constant spindle rotation Ω=8000 rpm along the straight line of 80 mm. Experimental verification and numerical simulation of the described case of the milling process with KUKA KR-270 robot using the algorithm shown in Figure 6 allows us to trace the evolution of machining force x,y-components for the whole process (Figure 11). The corresponding dynamic displacement of the tool around its current position on the trajectory is shown in Figure 12.
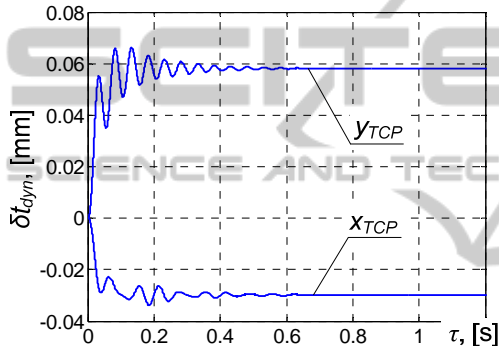

Figure 12: Evolution of the tool dynamic displacement δt_{dyn} that is composed from x_{TCP} and y_{TCP} components.
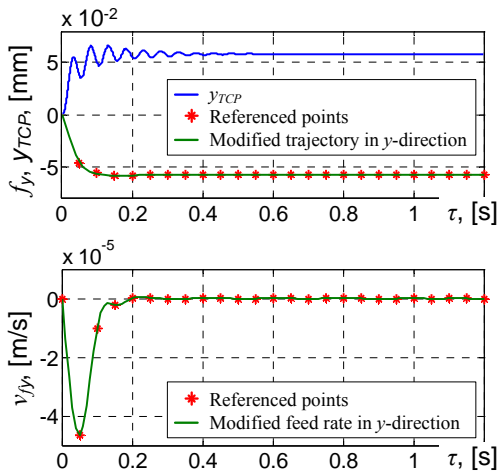

Figure 13: Modified trajectory f_y and corresponding feed rate v_{fy} in y-direction, computed based on the original dynamic displacement of the tool δt_{dyn}.

In accordance with the obtained results the system robot/machining process realize complex vibratory motion. The high frequency component of this motion (about 700 Hz, Figure 11) is related to the spindle ro-

tation and the number of tool teeth N_z. In certain cases such behavior can excites the dynamics of the robot (natural modes) but this study remains out the frame of the presented paper. On the contrary, the low frequency component of robot/tool motion (about 7 Hz, Figure 12), especially in the y-direction (that is perpendicular to the applied feed) influences directly the quality of final product. Such motion is related to the robot compliance and it can be compensated using the error compensation technique described in the paper. Hence, let us form the modified trajectory based on the dynamic displacement of the robot end-effector in the y-direction (Figure 13):

It should be stressed that the time step between referenced points of this modified trajectory is limited with the characteristics of the controller used in the robot (in the presented case this step is chosen 0.05 sec). The corresponding feed rate v_{fy} for the modified trajectory has been computed. So, this new data (feed f_y and feed rate v_{fy}) with the data defined in the beginning of this section allow us to compensate the trajectory error during machining caused by the robot compliance. The resulted compensated trajectory in the y-direction (in time domain) is presented in Figure 14.
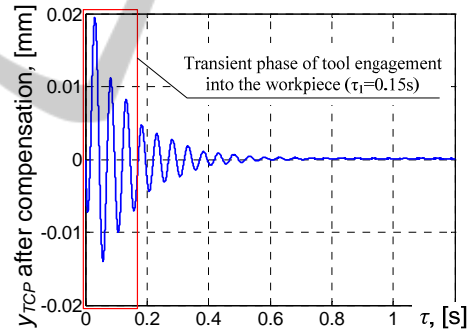

Figure 14: Evolution of the dynamic displacement obtained after involving the error compensation technique into the analysis of robotic milling process.

It should be noted that the part of the trajectory while machining tool is engaging into the workpiece does not have effect on the quality of final product (surface). During this stage the contact area between the tool and the workpiece is increasing progressively. Hence, at each instant of processing the cutter corrects the machining profile and eliminates trajectory errors produced during all previous instants. On the contrary, during the stage of machining with the fully engaged tool the trajectory in x,y-directions define directly the final machining profile and this part of trajectory is analyzed here (Figure 14). Comparison results presented in Figure 12 and Figure 14 are summarized in Table 2. So after applying error compensation technique the static deviation in y direction has been reduced from

0.058 mm to 0.00014 mm (99.8%). Maximum defilation in the machining profile has been reduced from 0.063 mm to 0.0047 mm (92.6%). Low frequency remained the same for both cases.

Table 2: Milling trajectory accuracy before and after compliance error compensation.

Performance measure	Original trajectory	Modified trajectory
Low frequency,[Hz]	6.70	6.70
Static deviation y_s, [mm]	58.1e-3	0.14e-3
Max deviation y_{MAX}, [mm]	63.2e-3	4.70e-3

Hence, obtained results show that the developed compliance error compensation allows us significantly increase the accuracy of the robotic-based machining.

7 CONCLUSIONS

In robotic-based machining, an interaction between the workpiece and technological tool causes essential deflections that significantly decrease the manufacturing accuracy. Relevant compliance errors highly depend on the manipulator configuration and essentially differ throughout the workspace. Their influence is especially important for heavy serial robots. To overcome this difficulty this paper presents a new technique for compensation of the compliance errors caused by technological process. In contrast to previous works, this technique is based on the non-linear stiffness model and the reduced elasto-dynamic model of the robotic based milling process.

The advantages and practical significance of the proposed approach are illustrated by milling with of KUKA KR270. It is shown that after error compensation technique significantly increase the accuracy of milling. In future the proposed technique will be integrated in a software toolbox.

ACKNOWLEDGEMENTS

REFERENCES

Alici G., Shirinzadeh B., 2005. Enhanced stiffness model ing, identification and characterization for robot manipulators. *Proceedings of IEEE Transactions on Robotics*, vol. 21, pp. 554–564.

Altintas Y., 2000. Manufacturing automation, metal cutting mechanics, machine tool vibrations and CNC design. *Cambridge University Press, New York*.

Brissaud D., Gouskov A., Paris H., Tichkiewitch S., 2008. The Fractional Model for the Determination of the Cutting Forces. *Asian Int. J. of Science and Technology - Production and Manufacturing*, vol. 1, pp.17-25.

Briot S., Pashkevich A., Chablat D. Reduced elastodynamic modelling of parallel robots for the computation of their natural frequencies. *13th World Congress in Mechanism and Machine Science*, 19 - 25 Juin, 2011, Guanajuato, Mexico.

Chen S., Kao I., 2000. Conservative Congruence Transformation for Joint and Cartesian Stiffness Matrices of Robotic Hands and Fingers. *The International Journal of Robotics Research*, vol. 19(9), pp. 835–847.

Dépincé P., Hascoët J-Y., 2006. Active integration of tool deflection effects in end milling. Part 2. Compensation of tool deflection, *International Journal of Machine Tools and Manufacture*, vol. 46, pp. 945-956

Dumas C., Caro S., Garnier S., Furet B., 2011. Joint stiffness identification of six-revolute industrial serial robots, *Robotics and Computer-Integrated Manufacturing*, vol. 27(4), pp. 881-888.

Eastwood S. J., Webb P., 2010. A gravitational deflection compensation strategy for HPKMs, *Robotics and Computer-Integrated Manufacturing*, vol. 26 pp. 694–702

Gong, C., Yuan J., Ni, J., 2000. Nongeometric error identification and compensation for robotic system by inverse calibration. *International Journal of Machine Tools & Manufacture*, vol. 40(14) pp. 2119–2137.

Kövecses J., Angeles J., 2007. The stiffness matrix in elastically articulated rigid-body systems. *Multibody System Dynamics*. vol. 18(2), pp. 169–184.

Laporte S., K'nevez J.-Y., Cahuc O., Darnis P., 2009. Phenomenological model for drilling operation. *Int. J. of Advanced Manufacturing Technology*, vol.40, pp.1-11.

Merchant M. E., 1945. Mechanics of metal cutting process. I-Orthogonal cutting and type 2 chip. *Journal of Applied Physics*, vol.16(5), pp.267–275.

Pashkevich A., Klimchik A., Chablat D., 2011. Enhanced stiffness modeling of manipulators with passive joints. *Mech. and Machine Theory*, vol. 46(5), pp. 662-679.

Ritou M., Garnier S., Furet B., Hascoet J.Y., 2006. A new versatile in-process monitoring system for milling, *Int. J. of Machine Tools & Manufacture*, 46/15:2026-2035.

Tlusty J., Ismail F., 1981, Basic non-linearity in machining chatter. *Annals of CIRP*, Vol.30/1, pp.299-304.

Tyapin I., Hovland G., 2009. Kinematic and elastostatic design optimization of the 3-DOF Gantry-Tau parallel kinamatic manipulator. *Modelling, Identification and Control*, vol. 30(2), pp. 39-56

Su H.-J., McCarthy J. M., 2006. A Polynomial Homotopy Formulation of the Inverse Static Analyses of Planar Compliant Mechanisms. *Journal of Mechanical Design*, vol. 128(4), pp. 776-786.